**Piezoelectric, elastic, structural and dielectric properties of the Si1-xGexO2 solid solution: A theoretical study.**



Kh. E. El-Kelany, A. Erba, Ph. Carbonniere, M. Rerat
Piezoelectric, elastic, structural and dielectric properties of the Si1-xGexO2 solid solution: A theoretical study.
JOURNAL OF PHYSICS. B, ATOMIC MOLECULAR AND OPTICAL PHYSICS (2014) 26

# Piezoelectric, Elastic, Structural and Dielectric Properties of the $Si_{1-x}Ge_xO_2$ Solid Solution: A Theoretical Study.

Khaled E. El-Kelany,[1,2,*] Alessandro Erba,[3] Philippe Carbonnière,[1] and Michel Rérat[1]

[1] *Equipe de Chimie Physique, IPREM UMR5254, Université de Pau et des Pays de l'Adour, 64000 Pau, France*

[2] *Chemistry Department, Faculty of Science, Minia University, Minia 61519, Egypt*

[3] *Dipartimento di Chimica and Centre of Excellence NIS (Nanostructured Interfaces and Surfaces), Università di Torino, via Giuria 5, IT-10125 Torino (Italy)*

(Dated: October 9, 2013)

We apply *ab initio* quantum mechanical techniques to the study of the solid solution $Si_{1-x}Ge_xO_2$ of $\alpha$-quartz where silicon atoms are progressively substituted with germanium atoms, to different extent as a function of the substitutional fraction $x$. For the first time, the whole range of substitution ($x$ = 0.0, 0.1$\overline{6}$, 0.$\overline{3}$, 0.5, 0.$\overline{6}$, 0.8$\overline{3}$, 1.0), including pure end-members $\alpha$-$SiO_2$ and $\alpha$-$GeO_2$, is here explored. An elongated supercell (doubled along the $c$ crystallographic axis) is built with respect to the unit cell of pure $\alpha$-quartz and a set of thirteen symmetry-independent configurations is considered; their structural, energetic, dielectric, elastic and piezoelectric properties are computed and analyzed. All the calculations are performed using a development version of the CRYSTAL09 program with a Gaussian-type-function, pseudopotential, basis set and the hybrid functional PBE0; all geometries are fully optimized at this level of theory. In particular, for each configuration, fourth-rank elastic and compliance tensors and third-rank *direct* and *converse* piezoelectric tensors are computed. It has already been shown that the structural distortion of the solid solution increases, almost linearly, as the substitutional fraction $x$ increases. The piezoelectric properties of the $Si_{1-x}Ge_xO_2$ solid solution are found to increase with $x$, with a similar quasi-linear behavior. The electromechanical coupling coefficients are enhanced as well and the linear trend recently predicted by Ranieri *et al.* [*Inorg. Chem.*, **50**, 4632 (2011)] can be confirmed from *ab initio* calculations. These doped crystals do represent good candidates for technological applications requiring high piezoelectric coupling and high thermal stability.

## I. INTRODUCTION

The low temperature phase of silica, $\alpha$-quartz, has a trigonal crystalline structure of symmetry group $P3_221$ (or $P3_121$), containing three $SiO_2$ formula units per unit cell. Its structure consists of sharing-corner $SiO_4$ tetrahedra. Among silica polymorphs, $\alpha$-quartz ($\alpha$-$SiO_2$ in the following) is the most stable form at ambient conditions (up to 3 GPa).[1] Upon heating at atmospheric pressure, $\alpha$-$SiO_2$ undergoes a phase transition at 846 K to $\beta$-$SiO_2$;[2] in the transition, silicon atoms are displaced by 0.03 nm and the crystalline system passes from trigonal to hexagonal with space group $P6_222$ (or $P6_422$).[3]

Due to its peculiar piezoelectric properties, $\alpha$-$SiO_2$ is widely applied in the electronic industry. However, its physical properties are severely reduced for applications requiring high thermal stability and high electromechanical coupling coefficients. These limitations are mainly due to the $\alpha$-$SiO_2$ to $\beta$-$SiO_2$ phase transition where the piezoelectric constant $d_{11}$ vanishes and $d_{14}$ remains the only non-zero component.[4]

Interestingly, piezoelectric properties of quartz homeotypes $A^{IV}O_2$ ($A^{IV}$ = Si, Ge) and $M^{III}X^{V}O_4$ ($M^{III}$ = B, Al, Ga, Fe and $X^{V}$ = P, As) are predicted to be much larger than that of quartz. All these materials crystallize in the same space group as $\alpha$-$SiO_2$ and then their structure can be described in terms of helical chains of adjacent tetrahedra along the $c$ axis.[5–10] The high piezoelectric performance of these $\alpha$-$SiO_2$ homeotypes is related to the degree of distortion in their crystal structure; the more distorted is the structure, the higher piezoelectric response is expected. This structural distortion can be described by two angles: the intertetrahedral bridging angle, $\theta$, and the tetrahedral tilting angle, $\delta$, which, in the case of undistorted tetrahedra, are geometrically related to each other by the following relation:[11] $\cos\theta = 3/4 - [\cos\delta + 1/(2\sqrt{3})]^2$. Tilting angle $\delta$ is an order parameter for the $\alpha$ - $\beta$ phase transition and corresponds to the rotation of the tetrahedra from their ideal position in $\beta$-$SiO_2$ where $\delta = 0$.[12] When the structure is distorted, $\theta$ and $\delta$ decreases and increases, respectively. A graphical definition of these two angles is given in Figure 1.

The electromechanical coupling coefficients represent the effectiveness with which a piezoelectric material converts electrical energy into mechanical energy or *vice versa*. It has recently been suggested that the electromechanical coupling coefficients depend linearly on the intertetrahedral $\theta$ angle.[12,13]

Among quartz homeotypes, $GaAsO_4$ ($\theta$ = 129.6 deg and $\delta$ = 26.5 deg)[8] and $\alpha$-$GeO_2$ ($\theta$ = 130 deg and $\delta$ = 25.7 deg)[5] have the most distorted structures. As a consequence, they also exhibit the highest electromechanical coupling coefficients (*i.e.* energy conversion efficiency), about 22 %. Furthermore, they show a very high degree of thermal stability since they do not undergo the $\alpha$ - $\beta$ phase transition.[12]

A series of solid solutions for $\alpha$-quartz homeotypes

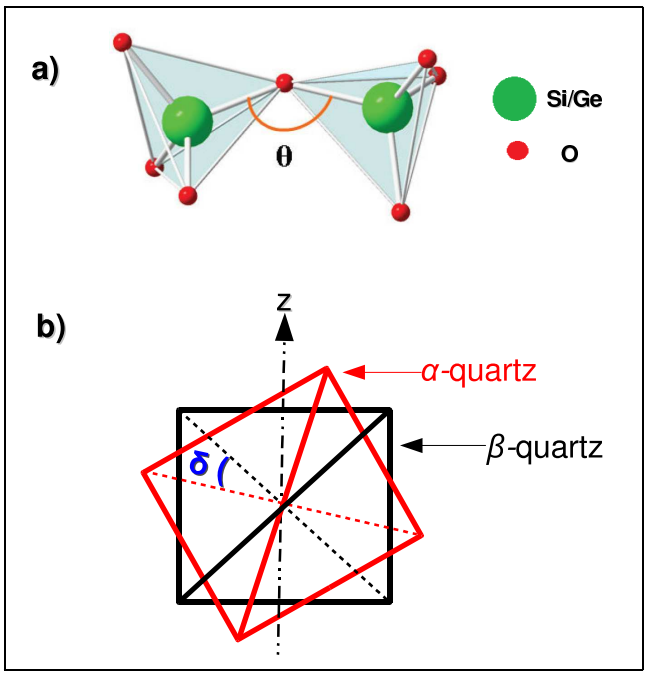


FIG. 1: (color online) Graphical definition of (a) the intertetrahedral bridging angle $\theta$ and (b) the tetrahedral tilting angle $\delta$ which is an order parameter for the $\alpha$ - $\beta$ phase transition in quartz.

has been studied both experimentally and theoretically: $SiO_2$-$GeO_2$,[14–18] $SiO_2$-PON (phosphorus oxynitride),[19] $SiO_2$-$AlPO_4$,[20] $AlPO_4$-$GaPO_4$,[21–25] $AlPO_4$-$AlAsO_4$,[21] $AlPO_4$-$FePO_4$,[26] $GaPO_4$-$FePO_4$.[27] The structural parameters and the piezoelectric properties of all these solid solutions are expected to vary as a function of the substitutional fraction $x$, thus representing an effective way for tuning such properties for specific technological applications.

Among these solid solutions, the $SiO_2$-$GeO_2$ system is probably the most promising; its phase diagram shows that the solubility of $\alpha$-$GeO_2$ into $\alpha$-$SiO_2$ can reach 31 % at 1000 K and 70 MPa, under hydrothermal conditions.[15] An attempt has been made to synthesize a series of $Si_{1-x}Ge_xO_2$ solid solutions of different chemical composition, as a function of $x$, by using hydrothermal and flux methods.[13,17,28] The first measurement of the piezoelectric response of one of these compositions ($Si_{0.93}Ge_{0.07}O_2$) indicates that the main piezoelectric constants, $d_{11}$ and $d_{14}$, exceed those of $\alpha$-quartz by 20 - 30 %. Furthermore, its $\alpha$ - $\beta$ phase transition temperature is found to be 1053 K, which is 207 K higher than that of pure quartz.[29]

In the present work, we apply *ab initio* quantum mechanical techniques to the simulation of several properties of the $Si_{1-x}Ge_xO_2$ system with different chemical composition. An elongated supercell (doubled along the $c$ crystallographic axis) is built with respect to the unit cell of pure $\alpha$-quartz where Si atoms are progressively substituted with Ge atoms. The whole range of substitution is here considered; beside the two end-members of the solid solution, $\alpha$-$SiO_2$ ($x = 0$) and $\alpha$-$GeO_2$ ($x = 1$), five intermediate compositions are taken into account: $x = 0.1\overline{6}$, $0.\overline{3}$, 0.5, $0.\overline{6}$ and $0.8\overline{3}$. Some intermediate compositions require different atomic configurations to be properly described; in some configurations, two Ge atoms are directly bridged one another by an O atom, while in others, Si atom(s) may lie between them. All possible symmetry-independent configurations are simulated for each substitutional fraction $x$; a total of thirteen symmetry-independent configurations are considered, overall.

A complete set of piezoelectric constants (elements of *direct* and *converse* third-rank piezoelectric tensors **e** and **d**, and electromechanical coupling coefficients k) and elastic constants (elements of the fourth-rank elastic $\mathbb{C}$ and compliance $\mathbb{S}$ tensors) is computed for each configuration. Electronic and nuclear contributions to the dielectric tensor $\epsilon$ are also computed. The effect on the electromechanical coupling constants of the chemical composition along the $Si_{1-x}Ge_xO_2$ solid solution series is analyzed. As a by-product, some insight can be gained about the influence of the chemical composition on structural and electronic properties.

All the calculations are performed using a development version of the CRYSTAL09 program[30,31] with a Gaussian-type-function, pseudopotential, basis set and the hybrid functional PBE0; all geometries are fully optimized at this level of theory.

The structure of the paper is as follows: the theoretical methodology adopted for the calculation of piezoelectric, elastic and dielectric tensors is presented in Section II; the definition and validation of the adopted computational setup is given in Section III; main results are presented and analyzed in Section IV where it is shown that the properties of the intermediate compositions vary smoothly and almost linearly with respect to the germanium content; conclusions are drawn in Section V.

## II. THEORETICAL METHODS

### A. Elastic Tensors Calculation

The elements of the fourth-rank elastic tensor $\mathbb{C}$ for 3D systems are usually defined as second energy density derivatives with respect to pairs of deformations:[32]

$$C_{vu} = \frac{1}{V}\left.\frac{\partial^2 E}{\partial\eta_v\partial\eta_u}\right|_0 , \qquad (1)$$

where $\boldsymbol{\eta}$ is the symmetric second-rank pure strain tensor, $V$ the equilibrium cell volume and Voigt's notation is used according to which $v, u = 1, \ldots, 6$ ($1 = xx$, $2 = yy$, $3 = zz$, $4 = yz$, $5 = xz$, $6 = xy$). An automated scheme for the calculation of $\mathbb{C}$ (and of $\mathbb{S} = \mathbb{C}^{-1}$, the compliance tensor) has been implemented in the CRYSTAL program

that exploits analytical gradients and compute numerically the second derivatives.[33,34]

### B. Piezoelectric Tensors Calculation

In the linear regime, *direct* **e** and *converse* **d** piezoelectric tensors describe the polarization **P** induced by strain $\boldsymbol{\eta}$ and the strain induced by an external electric field **E**, respectively:

$$\textit{direct}\ \text{effect} \qquad \mathbf{P} = \mathbf{e}\,\boldsymbol{\eta} \qquad \text{at constant field} \quad (2)$$

$$\textit{converse}\ \text{effect} \qquad \boldsymbol{\eta} = \mathbf{d}^T\mathbf{E} \qquad \text{at constant stress} \quad (3)$$

The *direct* and *converse* piezoelectric tensors are connected to each other: $\mathbf{e} = \mathbf{d}\,\mathbb{C}$ and $\mathbf{d} = \mathbf{e}\,\mathbb{S}$. Our approach consists in directly computing the intensity of polarization induced by strain. In CRYSTAL, the polarization can be computed either via localized Wannier functions or via the Berry phase (BP) approach.[35] The latter scheme is adopted in the automated implementation exploited here.[36]

The electromechanical coupling coefficients $k_{iv}$, which expresses the efficiency of transformation of mechanical into electrical energy, are defined as:[37,38]

$$k_{iv} = \frac{d_{iv}}{\sqrt{\epsilon^T_{ii} S_{vv}}} \quad \text{or} \quad k_{iv} = \frac{e_{iv}}{\sqrt{\epsilon^S_{ii} C_{vv}}}\ . \qquad (4)$$

Here $\boldsymbol{\epsilon}^T$ and $\boldsymbol{\epsilon}^S$ are the free stress and zero strain dielectric tensors, respectively. In this study, the electromechanical coupling coefficient is calculated using the right-hand side in expression (4), since in CRYSTAL the dielectric constant is calculated where the lattice parameters are fixed (constant strain).

### C. Dielectric Tensor Calculation

The electronic contribution to the polarizability and the dielectric tensor is evaluated through the Coupled Perturbed Hartree-Fock or Kohn-Sham (CPHF/KS) scheme[39] as adapted to periodic systems.[40] This is a perturbative, self-consistent method that describes the effect of an external electric field on the relaxation of the crystalline orbitals.

Additional details about the method and its implementation in the CRYSTAL program can be found elsewhere,[41–43] as well as recent example of applications.[36,44–48]

The total static dielectric tensor can be determined as follows:

$$\epsilon^0_{ij} = \epsilon^{\text{el}}_{ij} + \epsilon^{\text{vib}}_{ij} = \epsilon^{\text{el}}_{ij} + \frac{4\pi}{V}\sum_p \frac{Z_{p,i} Z_{p,j}}{\nu_p^2}\ , \qquad (5)$$

where $\epsilon^{\text{el}}_{ij}$ and $\epsilon^{\text{vib}}_{ij}$ are the electronic (clamped ion) and vibrational (ionic) contributions, $\nu_p$ is the phonon frequency of mode $p$, $V$ is the unit cell volume and $Z_p$ is the mass-weighted mode effective Born charge vector.[49]

## III. COMPUTATIONAL DETAILS

The calculations reported in this manuscript are performed with a development version of the CRYSTAL09 program.[30,31] An effective Durand preudopotential (PS) is used for describing core electrons.[50] Gaussian-type-functions are adopted for valence electrons: a PS-211G* basis set is used for Silicon, a PS-211G* one for Germanium and a PS-41G* one for Oxygen atoms, which have already been optimized in previous studies.[51]

The level of accuracy in evaluating the Coulomb and exact exchange infinite series is controlled by five parameters whose values are here set to $T_1 = T_2 = T_3 = T_4 = \frac{1}{2}T_5 = 8$.[30] The reciprocal space is sampled according to a regular sub-lattice with a shrinking factor of 8, corresponding to 65 independent **k** points in the first irreducible Brillouin zone (BZ). The DFT exchange-correlation contribution is evaluated by numerical integration over the unit cell volume. Radial and angular points of the integration grid are generated through Gauss-Legendre radial quadrature and Lebedev two-dimensional angular point distributions. A pruned grid with 99 radial and 1454 angular points is used (see the `XXLGRID` keyword in the CRYSTAL09 user's manual of Ref. 30). The numerical integration accuracy can be estimated by the error in the electronic charge per unit cell: $4.0 \times 10^{-6}|e|$ out of a total of 144 electrons per cell in $\alpha$-$GeO_2$, for instance.

The convergence of the self-consistent-field step is set to $10^{-10}$ hartree for both geometry optimizations and phonon frequency calculations. The fractional atomic coordinates and unit-cell parameters are optimized within a quasi-Newton scheme using analytical energy gradients combined with the Broyden-Fletcjer-Goldfarb-Shanno algorithm for Hessian updating.[52–55] The optimization convergence is checked on the root-mean-square (RMS) and maximum values of both gradients and nuclear displacements. The thresholds for the maximum and RMS forces are set to 0.00045 a.u. and 0.0003 a.u.; those for atomic displacements to 0.0018 a.u. and 0.0012 a.u., respectively.

Phonon vibrational calculations are performed within the harmonic approximation to the lattice potential.[56] Vibration frequencies at the $\Gamma$ point of the BZ are obtained by diagonalizing the dynamical mass-weighted Hessian matrix of the second derivatives of the total energy per cell with respect to pairs of atomic displacements in the reference cell. First derivatives are computed analytically, whereas second derivatives numerically (for more details see Ref. 57). Eckart's conditions are imposed in order to eliminate translational spurious contributions to the dynamical matrix.[58]

### A. One-electron Hamiltonian

Four different one-electron Hamiltonians are considered: the local density approximation (LDA) and a gen-

TABLE I: Effect of the adopted one-electron Hamiltonian on computed structural and electronic properties for $\alpha$-$SiO_2$ and $\alpha$-$GeO_2$. See text for a definition of the quantities reported.

| | LDA | PBE | B3LYP | PBE0 | Exp. |
|---|---|---|---|---|---|
| $\alpha$-$SiO_2$ | | | | | |
| $a = b$ (Å) | 4.777 | 4.921 | 4.939 | 4.898 | 4.916[59] |
| $c$ (Å) | 5.343 | 5.429 | 5.435 | 5.399 | 5.405[59] |
| $V$ (Å$^3$) | 105.62 | 113.88 | 114.83 | 112.18 | 113.13[59] |
| Si-$O_1$ (Å) | 1.629 | 1.629 | 1.619 | 1.616 | 1.607[59] |
| Si-$O_2$ (Å) | 1.637 | 1.634 | 1.623 | 1.621 | 1.614[59] |
| $O_1$-Si-$O_1$ (deg) | 107.11 | 108.45 | 108.67 | 108.48 | 108.93[59] |
| $O_1$-Si-$O_2$ (deg) | 112.40 | 111.19 | 110.63 | 110.89 | 110.52[59] |
| $\theta$ (deg) | 133.73 | 140.28 | 143.02 | 141.19 | 143.73[59] |
| $E_g$ (eV) | 7.0 | 7.4 | 10.1 | 10.6 | 8.9[60] |
| $\alpha$-$GeO_2$ | | | | | |
| $a = b$ (Å) | 4.932 | 5.130 | 5.174 | 5.101 | 4.985[61] |
| $c$ (Å) | 5.723 | 5.804 | 5.791 | 5.752 | 5.646[61] |
| $V$ (Å$^3$) | 120.57 | 132.30 | 134.24 | 129.61 | 121.50[61] |
| Ge-$O_1$ (Å) | 1.779 | 1.779 | 1.760 | 1.759 | 1.736[62] |
| Ge-$O_2$ (Å) | 1.788 | 1.784 | 1.765 | 1.764 | 1.741[62] |
| $O_1$-Ge-$O_1$ (deg) | 104.57 | 106.61 | 107.27 | 106.70 | 107.72[62] |
| $O_1$-Ge-$O_2$ (deg) | 115.03 | 112.98 | 111.96 | 112.55 | 110.49[62] |
| $\theta$ (deg) | 124.56 | 130.69 | 134.38 | 131.88 | 130.05[62] |
| $E_g$ (eV) | 3.4 | 3.6 | 6.0 | 6.4 | 5.7[63] |

eralized gradient approximation (GGA), namely Perdew-Burke-Ernzerhof (PBE),[64] to the density functional theory (DFT) and two hybrid schemes (namely B3LYP[65] and PBE0[66]) which include 20 and 25 % of exact HF exchange, respectively.

Table I shows the influence of the adopted one-electron Hamiltonian on computed structural and electronic properties of the two end-members $\alpha$-$SiO_2$ and $\alpha$-$GeO_2$. Lattice parameters, cell volume, bond lengths and angles, intertetrahedral angle $\theta$ and electronic band gap $E_g$ are reported and compared with experimental values. As regards lattice parameters, LDA underestimates them by 2.8 % for $\alpha$-$SiO_2$ and 1 % for $\alpha$-$GeO_2$ while PBE overestimates them by 1.7 % and 2.9 %, respectively. The B3LYP hybrid functional describes well the $\alpha$-$SiO_2$ structure, with a deviation of 0.5 %, but poorly the $\alpha$-$GeO_2$ structure (3.8 % of deviation from the experiment). The PBE0 hybrid functional is providing the best overall description of the structural features of the two end-members with deviations of 0.4 % and 2 %, respectively. Also the description of the $\theta$ intertetrahedral angle provided by hybrid functionals is satisfactory. The PBE0 hybrid functional is used in the following of the paper. Let us note that the electronic band gap obtained with PBE0 is slightly overestimated with respect to the experimental value and will then lead to slightly underestimated values for the optical dielectric tensor.

TABLE II: For any composition $x$, number $N_{\rm tot}$ of atomic configurations, number of $N_{\rm irr}$ symmetry-irreducible configurations among them, multiplicity $M$ and number of symmetry operators $N_{\rm ops}$ proper of each irreducible configuration.

| $x$ | $\frac{0}{6}$ | $\frac{1}{6}$ | $\frac{2}{6}$ | | | $\frac{3}{6}$ | | | $\frac{4}{6}$ | | | $\frac{5}{6}$ | $\frac{6}{6}$ |
|---|---|---|---|---|---|---|---|---|---|---|---|---|---|
| $N_{\rm tot}$ | 1 | 6 | 15 | | | 20 | | | 15 | | | 6 | 1 |
| $N_{\rm irr}$ | 1 | 1 | 3 | | | 3 | | | 3 | | | 1 | 1 |
| $M$ | 1 | 6 | 6 | 6 | 3 | 6 | 12 | 2 | 6 | 6 | 3 | 6 | 1 |
| $N_{\rm ops}$ | 12 | 2 | 2 | 2 | 4 | 2 | 1 | 6 | 2 | 2 | 4 | 2 | 12 |

## IV. RESULTS AND DISCUSSION

### A. Structural Model for Solid Solution

In the present study of the piezoelectric properties of the $Si_{1-x}Ge_xO_2$ solid solution, we want to consider the whole range of compositions. In particular, beside the two end-members, $\alpha$-$SiO_2$ ($x = 0$) and $\alpha$-$GeO_2$ ($x = 1$), we explicitly consider five intermediate compositions: $x = 0.1\overline{6}$, $0.\overline{3}$, 0.5, $0.\overline{6}$ and $0.8\overline{3}$. To do so, an elongated supercell (doubled along the $c$ crystallographic axis) is built with respect to the unit cell of pure $\alpha$-quartz. A new feature of the CRYSTAL program is exploited for finding automatically all the possible atomic configurations corresponding to any composition $x$.[67,68] For any substitutional fraction $x$, the program finds the total number $N_{\rm tot}$ of atomic configurations; a full symmetry analysis is then performed to find $N_{\rm irr}$ symmetry-irreducible configurations among them. To each irreducible atomic configuration, characterized by $N_{\rm ops}$ symmetry operators, a multiplicity $M$ is associated.

A total of thirteen symmetry-independent configurations are considered; their properties are illustrated in Table II. For the two pure phases, silicon (germanium) atoms are centered on equivalent $6a$ Wyckoff positions and only one atomic configuration is obviously possible, that is characterized by 12 symmetry operators. For the two compositions $x = \frac{1}{6} = 0.1\overline{6}$ and $x = \frac{5}{6} = 0.8\overline{3}$, there is one irreducible configuration out of six possible atomic configurations, each one invariant under 2 symmetry operators. Substitutional fractions $x = \frac{2}{6} = 0.\overline{3}$ and $x = \frac{4}{6} = 0.\overline{6}$ are described by a total of 15 atomic configurations, out of which 3 are found to be symmetry-independent: two of them with a multiplicity $M = 6$ (2 symmetry operators each) and one with multiplicity $M = 3$, with 4 symmetry operators. For the composition $x = \frac{3}{6} = 0.5$, 20 atomic configurations can be obtained; 3 are found to be symmetry-irreducible: the first one has 2 symmetry operators and a multiplicity $M = 6$, the second one has no symmetry at all and a multiplicity

TABLE III: Structural and energetic properties of the $Si_{1-x}Ge_xO_2$ solid solution series, as a function of the substitutional content $x$. Calculations are performed using the PBE0 hybrid functional. All data reported are per unit cell; $\Delta$E is the energy difference with respect to pure $\alpha$-quartz.

| | $SiO_2$ | $Si_{0.83}Ge_{0.17}O_2$ | $Si_{0.67}Ge_{0.33}O_2$ | $Si_{0.5}Ge_{0.5}O_2$ | $Si_{0.33}Ge_{0.67}O_2$ | $Si_{0.17}Ge_{0.83}O_2$ | $GeO_2$ |
|---|---|---|---|---|---|---|---|
| $\Delta$E (Ha/cell) | - | 0.1119 | 0.2235 | 0.3348 | 0.4459 | 0.5567 | 0.6672 |
| $a$ (Å) | 4.898 | 4.936 | 4.965 | 5.005 | 5.035 | 5.069 | 5.101 |
| $c$ (Å) | 5.400 | 5.459 | 5.516 | 5.575 | 5.633 | 5.692 | 5.752 |
| $c/a$ | 1.102 | 1.106 | 1.111 | 1.114 | 1.119 | 1.123 | 1.128 |
| $V$ (Å$^3$) | 112.2 | 115.2 | 118.1 | 120.9 | 123.8 | 126.6 | 129.6 |
| $\theta$ (deg) | 141.2 | 139.8 | 138.2 | 136.6 | 134.8 | 133.4 | 131.9 |
| $\delta$ (deg) | 18.6 | 19.7 | 20.9 | 22.1 | 23.4 | 24.5 | 25.6 |
| $\rho$ (g/cm$^3$) | 2.66 | 2.92 | 3.18 | 3.42 | 3.65 | 3.86 | 4.07 |
| Si-$O_1$ (Å) | 1.616 | 1.617 | 1.617 | 1.618 | 1.622 | 1.623 | - |
| Si-$O_2$ (Å) | 1.621 | 1.622 | 1.623 | 1.624 | 1.629 | 1.628 | - |
| Ge-$O_1$ (Å) | - | 1.750 | 1.750 | 1.751 | 1.755 | 1.756 | 1.759 |
| Ge-$O_2$ (Å) | - | 1.754 | 1.756 | 1.756 | 1.758 | 1.761 | 1.764 |

$M = 12$ while the third one is characterized by 6 symmetry operators and a multiplicity $M = 2$.

In the next tables, for each composition $x$, weighted average values will be reported over all the corresponding irreducible atomic configurations. In general, we find that, for a given substitutional fraction $x$, the variation of any considered property among the different irreducible configurations is quite small (lower than 1 %). For instance, the difference in the energy of the three irreducible configurations, in the case $x = \frac{2}{6}$, is less than $10^{-4}$ hartree and the difference in the lattice parameters and volume is lower than 0.003 Å and 0.3 Å$^3$, respectively.

### B. Structure and Energy

Structural and energetic properties of the $Si_{1-x}Ge_xO_2$ solid solution series are reported in Table III as a function of the composition $x$. The energy difference $\Delta$E with respect to pure $\alpha$-quartz, equilibrium lattice parameters $a$ and $c$, their ratio $c/a$, cell volume $V$, intertetrahedral bridging angle $\theta$, tetrahedral tilting angle $\delta$, density $\rho$ and several bond lengths and angles are reported. As mentioned above, all the reported data, for each composition $x$, are the weighted average values over all the corresponding irreducible configurations, where the weights in the averaging procedure are determined by the multiplicities $M$ given in Table II.

From the analysis of $\Delta$E, we can see how the inclusion of Ge atoms in pure $\alpha$-$SiO_2$ systematically destabilizes the structure, $\alpha$-$GeO_2$ being less stable than $\alpha$-$SiO_2$ by 0.6672 hartree/cell. Furthermore, it can be seen that the progressive substitution of each Si atom with a Ge atom increases the energy by about 0.111 ($\pm$0.001) hartree/cell at each substitutional step when passing from pure $\alpha$-$SiO_2$ to pure $\alpha$-$GeO_2$.

Along the $Si_{1-x}Ge_xO_2$ series, the cell volume $V$ increases quite linearly with the number of Ge atoms in the cell. Interestingly, also the distortion of the cell, that can be quantified by the $c/a$ ratio, increases linearly. The $c/a$ ratio, as well as $\theta$ and $\delta$ angles, reflects the intertetrahedral distortion in the helical chains; the ideal value of the $c/a$ ratio is 1.10 for pure $\alpha$-$SiO_2$ and 1.13 for pure $\alpha$-$GeO_2$ at room temperature.[69] The $c/a$ ratio, and $\theta$ and $\delta$ angles vary linearly with respect to the composition $x$, as observed experimentally.[13,17] Bond distances, X-$O_1$ and X-$O_2$ (with X = Si, Ge), vary regularly as a function of the composition. For instance, this can be observed in the systematic increase of the Si-O and Ge-O bond lengths, related to the internal distortion of the tetrahedra, as the Ge content increases.

### C. Elastic and Piezoelectric Properties

Before discussing into some detail the piezoelectric properties of the $Si_{1-x}Ge_xO_2$ solid solution, let us recall that direct and converse piezoelectricity measure the

TABLE IV: Elastic (in GPa) and compliance (in $TPa^{-1}$) constants of the $Si_{1-x}Ge_xO_2$ solid solution as a function of the composition $x$. Intertetrahedral bridging angle $\theta$ (in deg) and bulk modulus $B$ (in GPa) are also reported. Experimental data for $x = 0$ are from Ref. 69, for $x$ =0.07 from Ref. 29 and for $x = 1$ from Ref. 6. Calculations performed at PBE0 level.

| $x$ | | $\theta$ | Elastic Constants | | | | | | | Compliance Constants | | | | | | | $B$ |
|---|---|---|---|---|---|---|---|---|---|---|---|---|---|---|---|---|---|
| | | | $C_{11}$ | $C_{12}$ | $C_{13}$ | $C_{14}$ | $C_{33}$ | $C_{44}$ | $C_{66}$ | $S_{11}$ | $S_{12}$ | $S_{13}$ | $S_{14}$ | $S_{33}$ | $S_{44}$ | $S_{66}$ | |
| 0 | This study | 141.2 | 93.20 | 14.22 | 20.38 | 14.97 | 120.79 | 61.34 | 39.07 | 11.95 | -2.00 | -1.68 | -3.40 | 8.85 | 17.99 | 28.29 | 45.4 |
| | Exp. | 143.7 | 86.79 | 6.79 | 12.01 | 18.12 | 105.79 | 58.21 | 40.00 | 12.78 | -1.77 | -1.25 | -4.53 | 9.74 | 20.00 | 29.10 | 38[70] |
| 0.07 | Exp. | 142.6 | 85.5 | 10.38 | - | 16.3 | - | 57.2 | 37.5 | - | - | - | - | - | - | - | - |
| $0.1\overline{6}$ | This study | 139.8 | 83.62 | 15.56 | 20.89 | 12.23 | 114.06 | 54.86 | 33.82 | 13.49 | -2.55 | -2.01 | -3.57 | 9.57 | 19.85 | 32.32 | 42.7 |
| $0.\overline{3}$ | This study | 138.2 | 76.06 | 16.51 | 21.03 | 9.80 | 108.57 | 49.57 | 29.61 | 14.98 | -3.11 | -2.32 | -3.57 | 10.21 | 21.66 | 36.41 | 40.5 |
| 0.5 | This study | 136.7 | 69.80 | 17.49 | 21.21 | 7.79 | 104.24 | 44.87 | 26.09 | 16.52 | -3.77 | -2.62 | -3.54 | 10.78 | 23.57 | 40.71 | 38.8 |
| $0.\overline{6}$ | This study | 134.8 | 64.42 | 17.79 | 21.02 | 5.99 | 100.48 | 40.72 | 23.14 | 18.06 | -4.40 | -2.89 | -3.33 | 11.27 | 25.62 | 45.19 | 37.0 |
| $0.8\overline{3}$ | This study | 133.4 | 59.45 | 18.24 | 20.78 | 4.45 | 97.42 | 36.99 | 20.59 | 19.79 | -5.24 | -3.12 | -3.02 | 11.67 | 27.83 | 50.14 | 35.4 |
| 1 | This study | 131.9 | 54.73 | 18.08 | 20.75 | 3.15 | 94.68 | 33.69 | 18.31 | 21.71 | -6.02 | -3.44 | -2.60 | 12.07 | 30.20 | 55.54 | 33.7 |
| | Exp. | 130.0 | 64 | 22 | 32 | 2 | 118 | 37 | 21 | 19.25 | -4.68 | -3.95 | -1.29 | 10.62 | 27.17 | 47.87 | 32.8[71] |

Bulk modulus $B$ (GPa)$=\frac{1}{9}[a + 2b]$, where $a = 2C_{11} + C_{33}$ and $b = 2C_{13} + C_{12}$.

variation of polarization under a finite strain and the strain induced by an applied electric field, respectively. The two third-rank tensors associated with these properties, **e** and **d**, are connected to each other via the elastic $\mathbb{C}$ and compliance $\mathbb{S}$ fourth-rank tensors, according to the relations given in Section II B. For this reason we analyze first the elastic properties.

In Table IV we report, for each considered composition $x$, elastic constants $C_{vu}$, compliance constants $S_{vu}$, the intertetrahedral angle $\theta$ and the bulk modulus $B$ of the solid solution. Available experimental data are also reported, for pure end-members and for the $Si_{0.93}Ge_{0.07}O_2$ case. By comparing with the experiment, in these three cases, a good agreement is observed for most diagonal elements such as $C_{11}$, $C_{44}$ and $C_{66}$. Off-diagonal terms, such as $C_{12}$ and $C_{13}$, show a larger discrepancy which, however, can be expected since they have very small values and similar deviations are also found among different experiments.[6,10] The $C_{14}$ off-diagonal constant, though small, is in relatively good agreement with the experimental determinations.

If we look at the elastic properties of the $Si_{1-x}Ge_xO_2$ solid solutions of intermediate compositions, a very smooth connection is found between those of the end-members as a function of $x$, for all the elastic constants. An overall index of this smoothness is given by the bulk modulus $B$, reported in the last column of Table IV, which varies smoothly from 45.4 GPa for $\alpha$-$SiO_2$ to 33.7 GPa for $\alpha$-$GeO_2$. The good numerical accuracy of our approach for computing such properties can be inferred from inspection of the behavior of the very small $C_{14}$ off-diagonal constant which regularly varies from 14.97 GPa (18.12 GPa in the experiment) to 3.15 GPa (2.2 GPa in the experiment).

The overall effect of the progressive substitution of Ge atoms for Si atoms, is that of reducing the bulk modulus and, as a consequence, from our theoretical predictions, to decrease the values of all the diagonal elastic constants (a behavior that looks consistent). From the comparison with the experiments, the trends of two elastic constants show a discrepancy: i) the $C_{13}$ constant is theoretically predicted to be almost independent from the composition $x$, by passing from 20.38 GPa at $x = 0$ to 20.75 GPa at $x = 1$, whereas experimentally it becomes three times larger (from 12 GPa to 32 GPa); ii) the diagonal $C_{33}$ elastic constant is theoretically predicted to decrease from 120.79 GPa to 94.68 GPa while experimentally it grows in the opposite direction from 106 GPa to 118 GPa. In this respect, we should mention that the experimental determination of the elastic constants of the two end-members is not homogeneous since it has been performed in two separate experiments; our theoretical predictions seem to be more reliable in this case, at least as concerns the trend from $\alpha$-$SiO_2$ to $\alpha$-$GeO_2$ along the solid solution series.

In Table V, we report *direct* and *converse* piezoelectric constants, electronic and static dielectric constants (permittivity) and electromechanical coupling coefficients of the $Si_{1-x}Ge_xO_2$ solid solution, as a function of the substi-

TABLE V: *Direct* and *converse* independent piezoelectric constants, electronic and static dielectric constants (relative permittivity) and electromechanical coupling coefficients of the $Si_{1-x}Ge_xO_2$ solid solution, as a function of the composition $x$. Experimental data, when available, are reported for end-members. Calculations performed at PBE0 level.

| $x$ | 0 | | $0.1\overline{6}$ | $0.\overline{3}$ | 0.5 | $0.\overline{6}$ | $0.8\overline{3}$ | 1 | |
|---|---|---|---|---|---|---|---|---|---|
| | Calc. | (Exp.) | Calc. | Calc. | Calc. | Calc. | Calc. | Calc. | (Exp.) |
| Direct Piezoelectricity $e_{iv}$ ($C/m^2$) | | | | | | | | | |
| $e_{11}$ | 0.179 | (0.171)[a] | 0.197 | 0.208 | 0.222 | 0.229 | 0.236 | 0.241 | - |
| $e_{14}$ | -0.060 | (-0.041)[a] | -0.076 | -0.092 | -0.108 | -0.122 | -0.134 | -0.145 | - |
| $e_{26}$ | -0.184 | (-0.171)[a] | -0.196 | -0.208 | -0.218 | -0.228 | -0.234 | -0.240 | - |
| Converse Piezoelectricity $d_{iv}$ (pm/V) | | | | | | | | | |
| $d_{11}$ | 2.30 | (2.31)[a] | 2.89 | 3.46 | 4.08 | 4.70 | 5.49 | 6.31 | (4.04)[c] |
| $d_{14}$ | 0.18 | (0.73)[a] | 0.91 | 1.12 | 1.38 | 1.85 | 2.37 | 3.11 | (3.82)[c] |
| $d_{26}$ | -4.78 | (-4.62)[a] | -5.79 | -6.83 | -8.15 | -9.47 | -10.87 | -12.58 | - |
| Electronic Permittivity $\epsilon^{\infty}_{ij}$ | | | | | | | | | |
| $\epsilon^{\infty}_{11}$ | 2.13 | (2.36)[b] | 2.19 | 2.25 | 2.30 | 2.36 | 2.42 | 2.48 | (2.89)[d] |
| $\epsilon^{\infty}_{33}$ | 2.16 | (2.38)[b] | 2.22 | 2.29 | 2.35 | 2.42 | 2.49 | 2.60 | (2.99)[d] |
| Static Permittivity $\epsilon^{0}_{ij}$ | | | | | | | | | |
| $\epsilon^{0}_{11}$ | 4.21 | (4.43)[a] | 4.39 | 4.54 | 4.71 | 4.86 | 5.00 | 5.11 | (6.65)[e] |
| $\epsilon^{0}_{33}$ | 4.42 | (4.64)[a] | 4.60 | 4.73 | 4.90 | 5.06 | 5.19 | 5.26 | (7.43)[†] |
| Electromechanical Coupling $k_{iv}$ (%) | | | | | | | | | |
| $k_{11}$ | 9.61 | (10.23)[⋆] | 10.90 | 11.90 | 13.04 | 13.78 | 14.50 | 15.32 | - |
| $k_{14}$ | 3.94 | (2.63)[⋆] | 5.23 | 6.54 | 7.87 | 9.20 | 10.49 | 11.75 | - |
| $k_{26}$ | 15.26 | - | 17.10 | 19.07 | 20.92 | 22.86 | 24.52 | 26.38 | - |

[a] Ref. 72, [b] Ref. 73, [c] Ref. 10, [d] Ref. 74, [e] Ref. 75

[†] This value has been obtained from the oscillator strengths calculated from the eight Raman LO and TO phonon modes of Ref. 75.

[⋆] This value has been computed by Zeng *et al.*,[38] from experimental converse piezoelectric strain, free stress dielectric and compliance constants of Ref. 72.

tutional fraction $x$. Experimental data, when available, are reported for the two pure end-members. In particular, dielectric and piezoelectric properties of $\alpha$-$SiO_2$ have been extensively measured and a quite complete set of these constants is experimentally known. The agreement between our theoretical predictions and the experimental values is rather good for almost all quantities in the table. The only significant discrepancy is observed for the off-diagonal component, $d_{14}$, of the converse piezoelectric tensor and is due to the poor description of off-diagonal elastic and compliance constants (see again Table IV), probably affected by temperature effects, neglected in the calculations. Such a discrepancy, however, is fairly acceptable considering that the value of $d_{14}$ (0.18 pm/V) is quite small if compared with the other converse piezoelectric constants ($d_{11}$ = 2.30 pm/V and $d_{26} = -2d_{11}$ = -4.60 pm/V). According to the symmetry space group of the $\alpha$-quartz structure ($P3_221$), the piezoelectric constant $e_{26} = -e_{11}$ and $d_{26} = -2d_{11}$; deviations from these relations in Table V are due to numerical accuracy in the supercell calculations with reduced symmetry.

The comparison with experiments is much more difficult for the second end-member, $\alpha$-$GeO_2$, due to the fact that it does not exist in nature. Synthesizing and growing pure $\alpha$-$GeO_2$ crystals artificially is a difficult task so that the determination of its response properties is much less accurate than for $\alpha$-$SiO_2$.[76] For instance, the reported experimental value for the static dielectric constant $\epsilon^0_{33}$ has been indirectly calculated from longitudinal-optical, LO, and transverse-optical, TO, Raman frequencies, among which some are not very accurately measured (due to the presence of shoulders in the spectrum); the least-squares procedure used to obtain the static dielectric value is very sensitive to the starting frequency values.[75]

As regards the compositional effect on the piezoelectric response of the $Si_{1-x}Ge_xO_2$ solid solution, Table V clearly shows as both direct and converse piezoelectric constants regularly increase passing from pure $\alpha$-$SiO_2$ to pure $\alpha$-$GeO_2$ by progressively substituting Si atoms with Ge atoms, as suggested by Ranieri *et al.* a couple of years ago.[13]

For the dielectric response, it is seen from the table that the nuclear contribution to the permittivity is as large as the electronic one. This latter one reported in the work is small compared to the experimental one due to the overestimation of the electronic gap as mention in section III A. The static dielectric constant values, reported in the table, are used, via expression (4), for com-

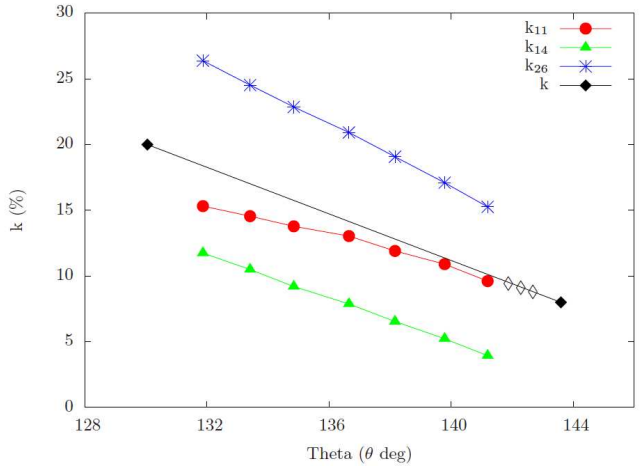


FIG. 2: (color online) Electromechanical coupling coefficients as a function of the intertetrahedral bridging angle $\theta$. The experimental values for pure end members (full black diamonds) are also reported.[13] In the experimental work, Ranieri *et al.* also predicted the coupling values for some intermediate compositions with small substitutional fraction $x$ assuming a linear behavior; these data are reported as empty black diamonds.

puting the electromechanical coupling coefficients ($k_{iv}$) that express the efficiency of a piezoelectric material in converting mechanical into electrical energy. Our computed values (via the second equality in equation 4) for $\alpha$-quartz are compared with data reported by Zeng *et al.*,[38] who computed them from experimental converse piezoelectric strain, free stress dielectric and compliance constants of Ref. 72, following the first equality in equation (4). Again, also the electromechanical coupling coefficients vary linearly along the $Si_{1-x}Ge_xO_2$ solid solution series and, in particular, they increase with $x$.

In Figure 2, we report the computed electromechanical coupling coefficients, $k_{11}$, $k_{14}$ and $k_{26}$, as a function of the intertetrahedral angle $\theta$ that, as discussed in the introduction, is related to the structural deformation of the $Si_{1-x}Ge_xO_2$ solid solution. From the figure, a perfect linear behavior is observed for both $k_{14}$ and $k_{26}$ coefficients while $k_{11}$ shows a slight deviation from linearity while increasing the content of Ge atoms. The experimental values for pure end members are obtained from the so-called AT-cut,[77] which almost, but not exactly, corresponds to the $k_{11}$ coefficient.[13] Our theoretical calculations can describe in a quite accurate way both the absolute values of these coefficients and their slope with respect to $\theta$.

Understanding how the piezoelectric, dielectric and elastic properties of the $Si_{1-x}Ge_xO_2$ solid solution can be tuned by varying the substitutional fraction of Ge atoms can prove extremely useful for designing materials with optimal properties for specific technological applications.

## V. CONCLUSIONS

The influence of the substitutional fraction $x$ in the $Si_{1-x}Ge_xO_2$ solid solution is theoretically investigated on a large variety of structural, dielectric, elastic and piezoelectric properties. For the first time, a full range of compositions $x$ (0.0, 0.1$\overline{6}$, 0.$\overline{3}$, 0.5, 0.$\overline{6}$, 0.8$\overline{3}$, 1.0), including pure $\alpha$-$SiO_2$ and $\alpha$-$GeO_2$ end-members, is considered. A set of thirteen symmetry-independent atomic configurations is studied. Accurate *ab initio* simulations are performed using the CRYSTAL program with the PBE0 global hybrid functional and atom-centered Gaussian-type-functions basis set.

Almost linear relationships are observed among the chemical composition $x$, structural distortion (given in terms of intertetrahedral angle $\theta$ and tilting angle $\delta$), elastic and piezoelectric properties. Such a linear behavior allows for simple tuning of several physical properties of interest by doping $\alpha$-quartz with different amounts of Ge atoms. In particular, piezoelectric properties are shown to be enhanced when increasing the concentration of Ge atoms. The electromechanical coupling coefficients, that express the efficiency of a piezoelectric material in converting mechanical into electrical energy, are also analyzed into some detail, as a function of the chemical composition and structural distortion.

### Acknowledgments

El-Kelany acknowledges the egyptian government for supporting his work at the Université de Pau et des Pays de l'Adour in France, with a grant. All the authors are grateful to Prof. Roberto Dovesi for useful discussions and to Dr. Valentina Lacivita and Prof. Philippe D'Arco for helping in the atomic configuration analysis.

* Electronic address: elkelanystar2008@yahoo.com

[1] R. Sosman, *The phases of silica*, vol. 1 of *The Phases of Silica* (Rutgers University Press, 1965).
[2] A. Wright and M. Lehmann, J. Solid State Chem. **36**, 371 (1981).
[3] W. Heywang, K. Lubitz, and W. Wersing, *Piezoelectricity Evolution and Future of a Technology* (Springer, Berlin, 2008).
[4] W. Cady, *Piezoelectricity*, vol. 1 (Dover Publications, 1964).
[5] J. Haines, O. Cambon, D. A. Keen, M. G. Tucker, and M. T. Dove, Appl. Phys. Lett. **81**, 2968 (2002).
[6] M. Grimsditch, A. Polian, V. Brazhkin, and D. Balitskii, J. Appl. Phys. **83**, 3018 (1998).
[7] P. Labéguerie, M. Harb, I. Baraille, and M. Rérat, Phys. Rev. B **81**, 045107 (2010).

[8] O. Cambon, J. Haines, G. Fraysse, J. Detaint, B. Capelle, and A. Van der Lee, J. Appl. Phys. **97**, 074110 (2005).
[9] J. Haines, O. Cambon, D. Cachau-Herreillat, G. Fraysse, and F. E. Mallassagne, Solid State Science **6**, 995 (2004).
[10] D. Balitskii, O. Sil'vestrova, V. Balitskii, Y. Pisarevskii, D. Pushcharovskii, and E. Philippot, Crystallography Reports **45**, 145 (2000).
[11] H. Grimm and B. Dorner, J. Phys. Chem. Solids **36**, 407 (1975).
[12] E. Philippot, P. Armand, P. Yot, O. Cambon, A. Goiffon, G. J. McIntyre, and P. Bordet, J. Solid State Chem. **146**, 114 (1999).
[13] V. Ranieri, S. Darracq, M. Cambon, J. Haines, O. Cambon, A. Largeteau, and G. Demazeau, Inorg. Chem. **50**, 4632 (2011).
[14] W. S. Miller, F. Dachille, E. C. Shafer, and R. Roy, Am. Mineral. **48**, 1024 (1963).
[15] E. C. Shafer, M. W. Shafer, and R. Roy, Z. Kristallogr. **107** (1956).
[16] B. A. Fursenko, V. A. Kirkinsky, and A. P. Rjaposov, *High-Pressure Science and Technology* (in: B. Vodar, P. Marteau (Eds.), Proc. 7th AIR-APT Int. Conf., Pergamon, Oxford, 1980).
[17] V. S. Balitsky, D. V. Balitsky, A. N. Nekrasov, and L. V. Balitskaya, J. Cryst. Growth **275**, 807 (2005).
[18] A. Largeteau, S. Darracq, and G. Goglio, Z. Naturforsch. **63b**, 739 (2008).
[19] J. Haines, C. Chateau, J. M. Léger, and R. Marchand, Ann. Chim. Sci. Mat. **26**, 209 (2001).
[20] I. V. Veksler, R. Thomas, and R. Wirth, Am. Mineral. **88**, 1724 (2003).
[21] D. Cachau-Herreillat, J. Bennazha, A. Goiffon, A. Ibanez, and E. Philippot, Eur. J. Solid State Inorg. Chem **29**, 1295 (1992).
[22] H. R. Xia, Z. K. Qin, W. Yuan, S. F. Liu, Z. Q. Zou, and J. R. Han, Cryst. Res. Technol. **32**, 783 (1997).
[23] H. Xia, J. Wang, L. Li, and Z. Zou, Prog. Cryst. Growth Char. Mater. **40**, 253 (2000).
[24] J. Haines, O. Cambon, G. Fraysse, and A. Van der Lee, J. Phys.: Condens. Mat. **17**, 4463 (2005).
[25] O. Cambon, J. Haines, M. Cambon, D. A. Keen, M. G. Tucker, L. Chapon, N. K. Hansen, M. Souhassou, and F. Porcher, Chem. Mater. **21**, 237 (2009).
[26] F. S. Mohamed, Adsopt. Sci. Technol. **20**, 741 (2002).
[27] M. Miclau, R. Bucur, P. Vlazan, R. Trusca, N. Miclau, and I. Grozescu, J. Opt. Adv. Mater. **9**, 2792 (2007).
[28] A. Lignie, D. Granier, P. Armand, J. Haines, and P. Papet, J. Appl. Cryst. **45**, 272 (2012).
[29] V. Balitsky, J. Detaint, P. Armand, P. Papet, and D. Balitsky, in *Frequency Control Symposium, 2007 Joint with the 21st European Frequency and Time Forum. IEEE International* (2007), pp. 704–710, ISSN 1075-6787.
[30] R. Dovesi, V. R. Saunders, C. Roetti, R. Orlando, C. M. Zicovich-Wilson, F. Pascale, B. Civalleri, K. Doll, N. M. Harrison, I. J. Bush, P. D'Arco, and M. Llunell, *CRYSTAL09 User's Manual*, Università di Torino, Torino (2010), http://www.crystal.unito.it.
[31] R. Dovesi, R. Orlando, B. Civalleri, C. Roetti, V. R. Saunders, and C. M. Zicovich-Wilson, Z. Kristallogr. **220**, 571 (2005).
[32] J. F. Nye, *Physical properties of crystals* (Oxford University Press, Oxford, 1957).
[33] W. F. Perger, J. Criswell, B. Civalleri, and R. Dovesi, Comput. Phys. Commun. **180**, 1753 (2009).
[34] A. Erba, A. Mahmoud, R. Orlando, and R. Dovesi, Phys. Chem. Minerals (2013), in press.
[35] Y. Noel, C. M. Zicovich-Wilson, B. Civalleri, P. D'Arco, and R. Dovesi, Phys. Rev. B **65**, 014111 (2001).
[36] A. Erba, Kh. E. El-Kelany, M. Ferrero, I. Baraille, and M. Rérat, Phys. Rev. B **88**, 035102 (2013).
[37] G. M. Bhalerao, O. Cambon, J. Haines, C. Levelut, A. Mermet, S. Sirotkin, B. Menaert, J. Debray, I. Baraille, C. Darrigan, and M. Rérat, Inorg. Chem. **49**, 9470 (2010).
[38] Y. Zeng, Y. Zheng, J. Xin, and E. Shi, Comput. Mat. Sci. **56**, 169 (2012).
[39] G. J. B. Hurst, M. Dupuis, and E. Clementi, J. Chem. Phys. **89**, 385 (1988).
[40] B. Kirtman, F. L. Gu, and D. M. Bishop, J. Chem. Phys. **113**, 1294 (2000).
[41] M. Ferrero, M. Rérat, R. Orlando, and R. Dovesi, J. Comp. Chem. **29**, 1450 (2008).
[42] M. Ferrero, M. Rérat, R. Orlando, and R. Dovesi, J. Chem. Phys. **128**, 014110 (2008).
[43] M. Ferrero, M. Rérat, R. Orlando, R. Dovesi, and I. J. Bush, J. Of Physics: Conference Series **117**, 012016 (2008).
[44] A. Erba, M. Ferrabone, J. Baima, R. Orlando, M. Rérat, and R. Dovesi, J. Chem. Phys. **138**, 054906 (2013).
[45] C. Carteret, M. De La Pierre, M. Dossot, F. Pascale, A. Erba, and R. Dovesi, J. Chem. Phys. **138**, 014201 (2013).
[46] V. Lacivita, A. Erba, Y. Noël, R. Orlando, P. D'Arco, and R. Dovesi, J. Chem. Phys. **138**, 214706 (2013).
[47] J. Baima, A. Erba, R. Orlando, M. Rérat, and R. Dovesi, J. Phys. Chem. C **117**, 12864 (2013).
[48] A. Erba and R. Dovesi, Phys. Rev. B **88**, 045121 (2013).
[49] X. Gonze and C. Lee, Phys. Rev. B **55**, 10355 (1997).
[50] P. Durand and J. C. Barthelat, Theor. Chim. Acta **38**, 283 (1975).
[51] E. Amzallag, Ph.D. thesis, Université de Pau et des Pays del'Adour (2007).
[52] C. G. Broyden, J. Inst. Math. Appl. **6**, 76 (1970).
[53] R. Fletcher, Comput. J. **13**, 317 (1970).
[54] D. Goldfarb, Math. Comput. **24**, 23 (1970).
[55] D. F. Shanno, Math. Comput. **24**, 647 (1970).
[56] C. M. Zicovich-Wilson, F. Pascale, C. Roetti, V. R. Saunders, R. Orlando, and R. Dovesi, J. Comp. Chem. **25**, 1873 (2004).
[57] F. Pascale, C. M. Zicovich-Wilson, R. Orlando, C. Roetti, P. Ugliengo, and R. Dovesi, J. Phys. Chem. B **109**, 6146 (2005).
[58] C. Eckart, Phys. Rev. **47**, 552 (1935).
[59] L. Levien, C. T. Prewitt, and D. J. Weidner, Am. Mineral. **65**, 920 (1980).
[60] E. Calabrese and W. B. Fowler, Phys. Rev. B **18**, 2888 (1978).
[61] J. D. Jorgensen, J. of Applied Physics **49**, 5473 (1978).
[62] J. Haines, O. Cambon, E. Philippot, L. Chapon, and S. Hull, J. Solid State Chem. **166**, 434 (2002).
[63] C. V. Ramana, G. Carbajal-Franco, R. S. Vemuri, I. B. Troitskaia, S. A. Gromilov, and V. V. Atuchin, Materials Science and Engineering: B **174**, 279 (2010).
[64] J. P. Perdew, K. Burke, and M. Ernzerhof, Phys. Rev. Lett. **77**, 3865 (1996).
[65] A. D. Becke, Phys. Rev. A **38**, 3098 (1988).
[66] C. Adamo and V. Barone, J. Chem. Phys. **110**, 6158 (1999).
[67] S. Mustapha, P. D'Arco, M. De La Pierre, Y. Noël, M. Ferrabone, and R. Dovesi, J. Phys.: Condens. Matter

**25**, 105401 (2013).
[68] P. D'Arco, S. Mustapha, M. Ferrabone, Y. Noël, M. De La Pierre, and R. Dovesi, J. Phys.: Condens. Matter **25**, 355401 (2013).
[69] E. Philippot, D. Palmier, M. Pintard, and A. Goiffon, J. Solid State Chem. **123**, 1 (1996), ISSN 0022-4596.
[70] C. Sevik and C. Bulutay, J. Mater. Science. **42**, 6555 (2007), ISSN 0022-2461.
[71] S. Kawasaki, O. Ohtaka, and T. Yamanaka, Physics and Chemistry of Minerals **20**, 531 (1994), ISSN 0342-1791.
[72] R. Bechmann, Phys. Rev. **110**, 1060 (1958).
[73] F. Gervais and B. Piriou, Phys. Rev. B **11**, 3944 (1975).
[74] D. Balitsky, V. Balitsky, D. Pushcharovsky, G. Bondarenko, and A. Kosenko, J. of Crystal Growth **180**, 212 (1997).
[75] J. F. Scott, Phys. Rev. B **1**, 3488 (1970).
[76] D. Balitsky, V. Balitsky, Y. V. Pisarevsky, E. Philippot, O. Y. Silvestrova, and D. Y. Pushcharovsky, in *Annales de Chimie Science des Materiaux* (Elsevier, 2001), vol. 26, pp. 183–192.
[77] C. S. Lam, Y. J.Chris, and S. M. Wang, in *Symposium on Piezoelectricity, Acoustic Waves, and Device Applications* (2008)